RESEARCH ARTICLE

P. Gerontakos · T. Lee

Near-field tip vortex behind a swept wing model

Abstract The near-field flow structure of a tip vortex behind a sweptback and tapered NACA 0015 wing was investigated and compared with a rectangular wing at the same lift force and $Re = 1.81 \times 10^5$. The tangential velocity decreased with the downstream distance while increased with the airfoil incidence. The core radius was about 3% of the root chord c_r, regardless of the downstream distance and α for $\alpha < 8°$. The core axial velocity was always wake-like. The core Γ_c and total Γ_o circulation of the tip vortex remained nearly constant up to $x/c_r = 3.5$ and had a Γ_c/Γ_o ratio of 0.63. The total circulation of the tip vortex accounted for only about 40% of the bound root circulation Γ_b. For a rectangular wing, the axial flow exhibited islands of wake- and jet-like velocity distributions with $\Gamma_c/\Gamma_o = 0.75$ and $\Gamma_o/\Gamma_b = 0.70$. For the sweptback and tapered wing tested, the inner region of the tip vortex flow exhibited a self-similar behavior for $x/c_r \geq 1.0$. The lift force computed from the spanwise circulation distributions agreed well with the force-balance data. A large difference in the lift-induced drag was, however, observed between the wake integral method and the inviscid lifting-line theory.

List of symbols

AR	Aspect ratio (b^2/S)
b	(Semi-)wing span
c	Chord of rectangular wing
c_r	Root chord
c_t	Tip chord
C_D	Drag coefficient without wing tip effects
C_{Di}	Lift-induced drag coefficient ($D_i/0.5\rho u_\infty^2 S$)
$C_{D,3\text{-}D}$	Drag coefficient of a 3-D wing configuration
C_L	Lift coefficient without wing tip effects ($L/0.5\rho u_\infty^2 S$)
$C_{L,3\text{-}D}$	Lift coefficient of a 3-D wing configuration
D	Drag without wing tip effects
$D_{3\text{-}D}$	Drag of a 3-D wing configuration
D_i	Lift-induced drag
L	Lift
p	Local static pressure
p_∞	Free-stream static pressure
r	Radial position
r_o	Vortex outer radius
r_c	Vortex core radius
Re	Reynolds number ($u_\infty c_r/v$ or $u_\infty c/v$)
S	Wing area
u	Axial mean velocity
u_c	Core axial velocity
u_∞	Free-stream velocity
v	Transverse mean velocity
v_θ	Tangential velocity
w	Spanwise mean velocity
x	Streamwise or axial direction
y	Normal direction
z	Spanwise direction
ρ	Fluid density
v	Fluid kinematic viscosity
ζ	Streamwise vorticity ($\partial w/\partial y - \partial v/\partial z$)
Γ	Circulation or vortex strength
Γ_b	Bound root circulation
Γ_c	Core circulation
Γ_o	Total circulation
α	Angle of attack
α_{ss}	Static-stall angle
λ	Taper ratio (c_t/c_r)
ψ	Stream function
ϕ	Velocity potential
σ	A source term in Eq. 6 ($\partial v/\partial y + \partial w/\partial z$)

P. Gerontakos · T. Lee (✉)
Department of Mechanical Engineering,
McGill University,
Quebec, Canada
E-mail: tim.lee@mcgill.ca

1 Introduction

The counter-rotating longitudinal vortices generated by aircraft wing tips, because of their hazardous effects on flight safety, continue to be of concern to the aviation industry and aircraft manufacturers alike. Moreover, tip vortices shed from helicopter rotor blades and propellers interact with the following blades causing rotor noise and vibration. Extensive investigations have been conducted to improve the understanding of the tip vortex structure and its dissipation or persistence, as well as its control. However, unlike the usual void of experimental data, a substantial effort has been invested in developing theoretical and numerical models for the roll-up process of tip vortices (Hoffmann and Joubert 1963; Batchelor 1964; Moore and Saffman 1973; Williams 1974; Phillips 1981; Green and Acosta 1991; Zeman 1995; Spalart 1998; Brune 1994; Kusunose 1997). The bulk of the experimental effort has been directed mainly toward finding the rate of change of the tangential velocity and the strength of trailing vortices in the mediate or far-field regions. Only limited experiments (Francis and Katz 1988; McAlister and Takahashi 1991; Shekarriz et al. 1993; Devenport et al. 1996; Chow et al. 1997; Ramaprian and Zheng 1997; Birch and Lee 2004), primarily restricted to wings with simple rectangular span loadings, have been conducted to investigate the dynamics of the initial roll-up of a tip vortex around the wing tip and its subsequent development in the near field of a wing. Measurements of the tip vortex behind a swept and tapered wing are even more limited (e.g. El-Ramly et al. 1976; Orloff and Ciffone 1974; Ozger et al. 2001).

Among the representative near-field tip vortex investigations, Francis and Kennedy (1979) measured the mean velocity and vorticity fields around a rectangular NACA 64009 wing, with an aspect ratio AR of 1.5, by using both a cross-hot-wire probe and flow visualization techniques at $Re = 2.4 \times 10^5$ and an angle of attack α of 4°. The measurements at the wing tip region showed that the properly non-dimensionalized characteristic vorticity distribution in the region was independent of α. Recently, Devenport et al. (1996) investigated the vortex structure in the range of $x/c = 4$–29 chord lengths downstream of a NACA 0012 airfoil with a blunt tip and an AR of 4.33 at $Re = 5.3 \times 10^5$ by using a miniature four-sensor hot-wire probe mainly at $\alpha = 5°$, and showed a deficit profile of approximately 84% of the free-stream velocity. Also, the flow outside the core was dominated by the remainder of the wing wake, which wound into an ever-increasing spiral, and the turbulence stress levels varied along the wake spiral in response to the varying rate of strain imposed by the vortex. Chow et al. (1997) investigated the tip vortex flow of a NACA 0012 airfoil model with a rounded tip (up to $x/c = 0.678$) and an AR of 1.333 at $Re = 4.6 \times 10^6$ and $\alpha = 10°$ by using a seven-hole pressure probe and a triple hot-wire probe, and indicated a high-level of axial velocity excess of approximately $1.7u_\infty$ at all measurement locations.

Chow et al. (1997) also reported that the vortex flow was found to be turbulent in the near field (as high as 24% rms velocity), and the turbulence decayed quickly with streamwise distance because of the stabilizing effect of the nearly solid body rotation of the vortex-core mean flow. Ramaprian and Zheng (1997) observed no axial velocity excess for a tip vortex generated by a square-tipped, rectangular NACA 0015 wing at $Re = 1.8 \times 10^5$ and $\alpha = 10°$ up to $x/c = 3.3$ using a three-component laser Doppler anemometer. Ramaprian and Zheng also observed that the roll-up of the separated shear layers took place quite quickly and the inner part of the three-dimensional vortex became nearly axisymmetric within a distance of about two chord lengths downstream of the trailing edge. Also, the mean flow properties in the inner part of the nearly axisymmetric tip vortex in the near field began to exhibit a universal structure of conceptual asymptotic trailing vortices. Most recently, Birch and Lee (2004) examined the flow structure of a tip vortex both along the tip and in the near field (up to $x/c = 2.5$) behind a square-tipped, rectangular NACA 0015 wing at $Re = 2.10 \times 10^5$ for $\alpha = 4$–20° by using a miniature seven-hole pressure probe and a cross-hot-wire probe. A local peak value of the circulation of the vortex was observed at $x/c = 0.05$ (immediately downstream of the wing trailing edge) and remained virtually unchanged up to $x/c = 2.5$. Also, depending on α, the streamwise core flow could be wake or jet-like. The lift-induced drag coefficient, based on the vorticity distributions inferred from the measured crossflow fields, was computed and was also compared with the wind-tunnel force-balance data. However, despite much work on the tip vortex behind a rectangular wing, the characterization of the tip vortex in the near field behind a sweptback and tapered wing is limited.

The objective of the present experiment was to investigate the 3-D flow structure of the tip vortex in the near field behind a sweptback and tapered NACA 0015 wing by using a miniature seven-hole pressure probe at $Re = 1.81 \times 10^5$. Special attention was given to the effects of airfoil incidence and downstream distance on the behavior and variation of the crossflow and axial velocity and vorticity distributions, and the strength and size of the tip vortex. Lift and lift-induced drag were also computed and were compared with the force-balance data and also the inviscid lifting-line theory. These measurements were also compared with a square-tipped, rectangular wing at the same lift and Re conditions so as to signify the geometric, or platform, effects on the behavior of a tip vortex.

2 Experimental apparatus and methods

The experiment was carried out in the recently constructed low-turbulence 0.9×1.2×2.7 m suction-type subsonic wind tunnel at McGill University with a free-stream turbulence intensity of 0.03% at 35 m/s. An

untwisted sweptback, tapered wing, made of solid aluminum, with an aspect ratio AR of 3.654, a taper ratio λ of 0.375, a semi-span b of 51 cm, and a wing area S of 713 cm^2, was used as the test model (Fig. 1a). The surface roughness of the wing model was estimated to be less than 51 μm. Also shown in Fig. 1a are the locations of the downstream vortex-flow measurement planes (denoted by the dashed lines). The sweep angle at 0.25-chord location was set at 24°. The root chord c_r was 20.3 cm and the tip chord c_t was 7.6 cm. The square-tipped wing had a NACA 0015 section throughout. The wing model was mounted horizontally at the center of the wind tunnel test section. A circular endplate of 50 cm diameter with a sharp leading edge was fitted to the one end, located 10 cm from the sidewall of the test section, of the wing model to isolate the free-end effects. The origin of the coordinate system was located at the trailing edge of the root of the wing with the x, y, and z axes in the streamwise, transverse, and spanwise directions, respectively. Mean tip-vortex flow velocities (u, v, and w) were measured in planes perpendicular to the free-stream velocity at six distances downstream of the trailing edge of the wing based on the root chord of the wing; $x/c_r = 0.625$, 1, 1.5, 2, 2.75, and 3.5 (or $x/c_t = -0.066$, 0.934, 2.267, 3.61, 5.601, and 7.601) for $\alpha = 8°$ by using a miniature seven-hole pressure probe with an outside diameter of 2.6 mm. The probe was calibrated in situ, following the calibration procedures described by Wenger and Devenport (1999), before the installation of the model. Eight pressure transducers (seven for the probe and one for tunnel reference total pressure) were used to maximize the data rate of the probe measurement system at each measurement location. The pressure signals were sampled at 500 Hz, with a sampling time of 5 s, and were recorded on a PC through a 16-bit A/D converter board. Probe traversing was achieved through a custom-built computer-controlled traversing system. The variation of the vortex flow quantities with α was also examined for $\alpha = 4$–14° at $x/c_r = 2.75$. Each data plane taken in the near field of the wing models had 33×85 measuring grid points with an increment of $\Delta y = \Delta z = 3.2$ mm, except along the span of the wing where $\Delta z = 6.4$ mm. A finer $\Delta y = \Delta z = 1.6$ mm was also used in the determination of the vortex-core characteristics. Figure 2a shows the adaptive grid method employed in the present experiment.

Note that due to the limitation of the probe traversing mechanism, the present wake survey region did not encompass the entire wing; only 85% of the wing wake was measured. The free-stream velocity was fixed at 13.84 m/s, which rendered a root-chord Reynolds number of 1.81×10^5. The lift-induced drag coefficients C_{Di} were also computed, based on the vorticity distributions inferred from the measured crossflow fields, and were compared with the wind-tunnel force-balance data and the inviscid lifting-line theory as well. These measurements were also compared with the vortex flow quantities observed behind a square-tipped rectangular wing (with $c = 20.3$ cm, $b = 50.8$ cm, $S = 1103.2$ cm^2, and

AR = 2.5) at the same lift ($C_{L,3\text{-}D} = 0.73$) and Re conditions. No boundary-layer transition strips were placed on the upper and lower surfaces of the wing models. Also, no wind tunnel wall corrections were made to the present measurements.

For lift and drag measurements, the wing models were mounted vertically on an external two-component force balance located below the wind tunnel (Fig. 1b). The wing model was mounted vertically between two 0.45×60×60 cm aluminum endplates with sharp leading edges. The bottom plate was fixed to the bottom wall of the test section and an aerodynamic fairing was placed around the shaft to isolate it from the tunnel flow. The top endplate was mounted on the top wall of the test section. The gaps between the airfoil and the endplates were kept at less than 1 mm to minimize leakage of flow through the gaps. Details of the force-balance system are given in Birch and Lee (2004). The lift and drag coefficients of the wing models without the tip effects will hereafter be referred to as C_L and C_D, respectively. Also, by removing the top endplate, the total lift coefficient $C_{L,3\text{-}D}$ and drag coefficient $C_{D,3\text{-}D}$ of a 3-D wing configuration were obtained. The maximum experimental uncertainties in the results reported have been estimated to be (Birch and Lee 2004): mean velocity 3.5%, vorticity component 8%, vortex radius 4%, and velocity fluctuation 3%. The uncertainty in C_L, C_D, and C_{Di} determinations were ± 0.01, ± 0.007, and 5%, respectively.

It is also known that the lateral excursions to which a trailing vortex is prone when situated in a stream containing ambient turbulence has long caused problems in measurement of vortex characteristics, and that the meander amplitude is linearly proportional to the level of free-stream turbulence and to the downstream distance from the generating lifting surface. In the present low-turbulence wind tunnel, the meander amplitude was greatly reduced because of the reduction in stream turbulence. The vortex meandering in the near field behind the generating wing was examined by using the correlation technique/criteria employed by Chow et al. (1997). The meandering of the vortex was found to be small and did not contribute appreciably to the present measurements.

3 Results and discussion

3.1 Vortex flow characteristics

Figure 2b, c displays the representative crossflow velocity vectors overlaid with the mean axial velocity u/u_∞ contours, and the mean streamwise or axial vorticity $\zeta c_r/u_\infty$ contours of the whole wake region behind the sweptback and tapered wing at $x/c_r = 2$ for $\alpha = 8°$. The dashed lines denote the trailing edge of the wing. Two distinct flow structures can be clearly seen in the flow field: the wing wake and the trailing tip vortex. The majority of the vorticity was found to be located in the
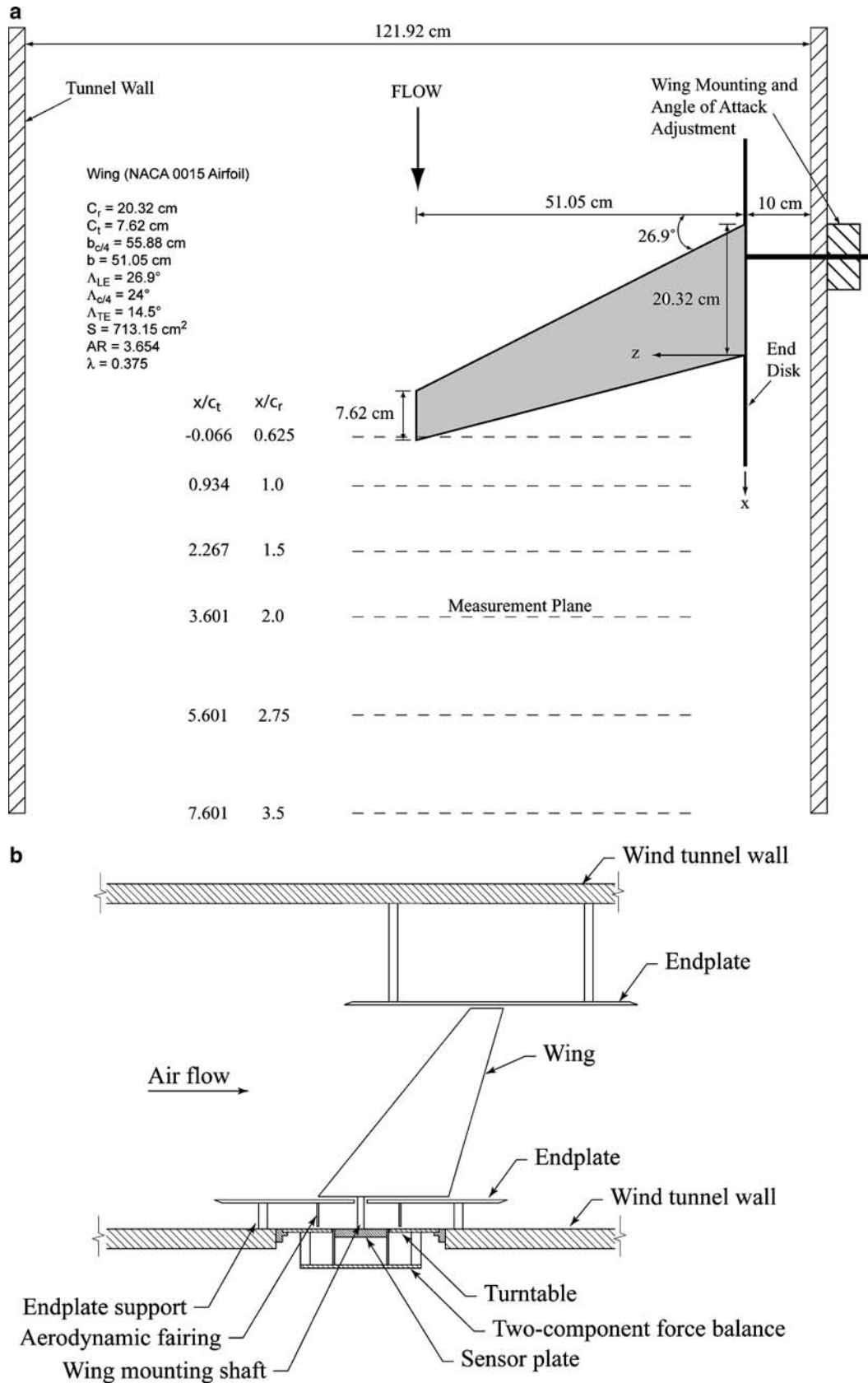
Fig. 1 Schematic of **a** sweptback and tapered wing model and **b** force-balance measurement system
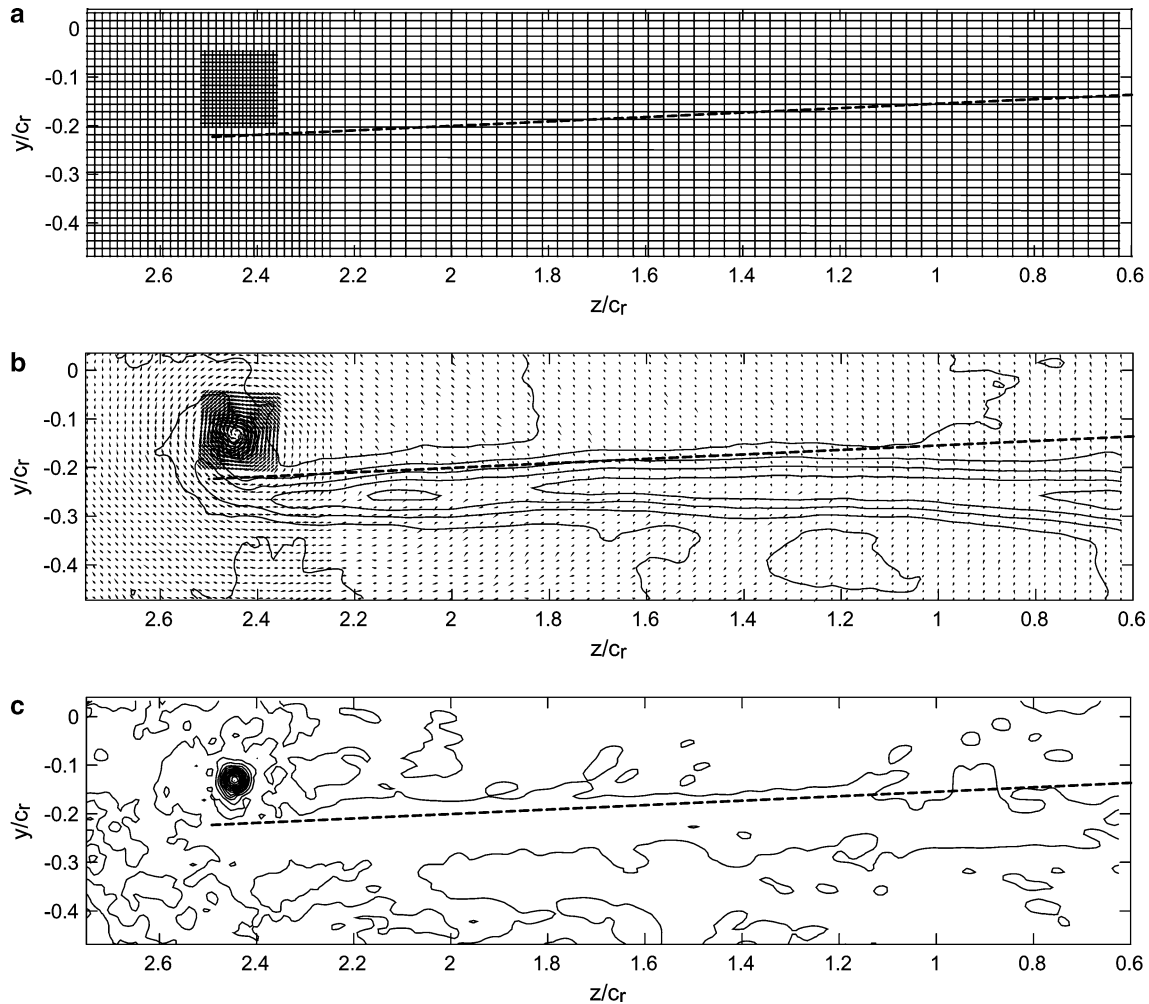
Fig. 2 **a** Adaptive grid and the whole measurement region. Typical non-dimensional **b** crossflow velocity vectors overlaid with mean axial velocity contours, and **c** axial vorticity contours at $x/c_r = 2$ for $\alpha = 8°$

small and concentrated core of the tip vortex. Outside the wake and tip vortex regions, the vorticity was essentially zero and the axial velocity attained the value of the free stream. The vw-vectors suggest a typical vortex circulation (Fig. 2b). Moreover, the center of this circulation appeared to be inboard from the tip and above the wing (Fig. 2c). It is important to note that for a square-tipped, untwisted, sweptback and tapered NACA 0015 wing (with $AR = 3.654$ and $\lambda = 0.375$) positioned at $\alpha = 8°$, the majority of the axial vorticity exhibited axisymmetric and circular shapes (except the outer flow region) at $x/c_r = 2$. Details of the nature of the tip vortex flow quantities, including the tangential velocity v_θ, ζ, and u, and the vortex size, at different downstream locations and α are presented in Figs. 3, 4, 5, 6, and 7.

Figure 3a shows that for $\alpha = 8°$ the flow consisted of a small concentrated vortex core (of a radius of $0.03c_r$ or $0.08c_t$) at $x/c_r = 0.625$. Outside the core the flow structure was dominated by the remainder of the wing wake, which wound into an ever-increasing spiral. The flow outboard of the wing followed nearly a circumferential path about the vortex center; however, inboard, there was a strong radial flow away from the vortex center. The iso-vorticity contour shows a relatively asymmetric or developing pattern (especially in the outer flow region) at this location; the vortex was not fully rolled up and a considerable remnant of the wake was still visible. Further downstream, the tangential and axial velocity and vorticity distributions were attaining axisymmetry and the axial velocity deficit was reducing. For $x/c_r > 0.625$ (Fig. 3b, c), a well-developed axisymmetric tip vortex with axisymmetric v_θ profiles and ζ distributions clearly existed, especially in the inner region of the vortex. The degree of axisymmetry became more pronounced with the downstream distance with no noticeable change in the level of the vorticity contours. It is significant to note that for $1 \leq x/c_r \leq 3.5$ (or $0.934 \leq x/c_t \leq 7.601$) studied, the majority of the vortex roll-up, except the outer flow region, was nearly completed; this can be demonstrated from the observed axisymmetric distributions of v_θ, ζ, and u, and, in particular, the coincidence of the point of minimum axial velocity deficit with the vortex center (located by the maximum
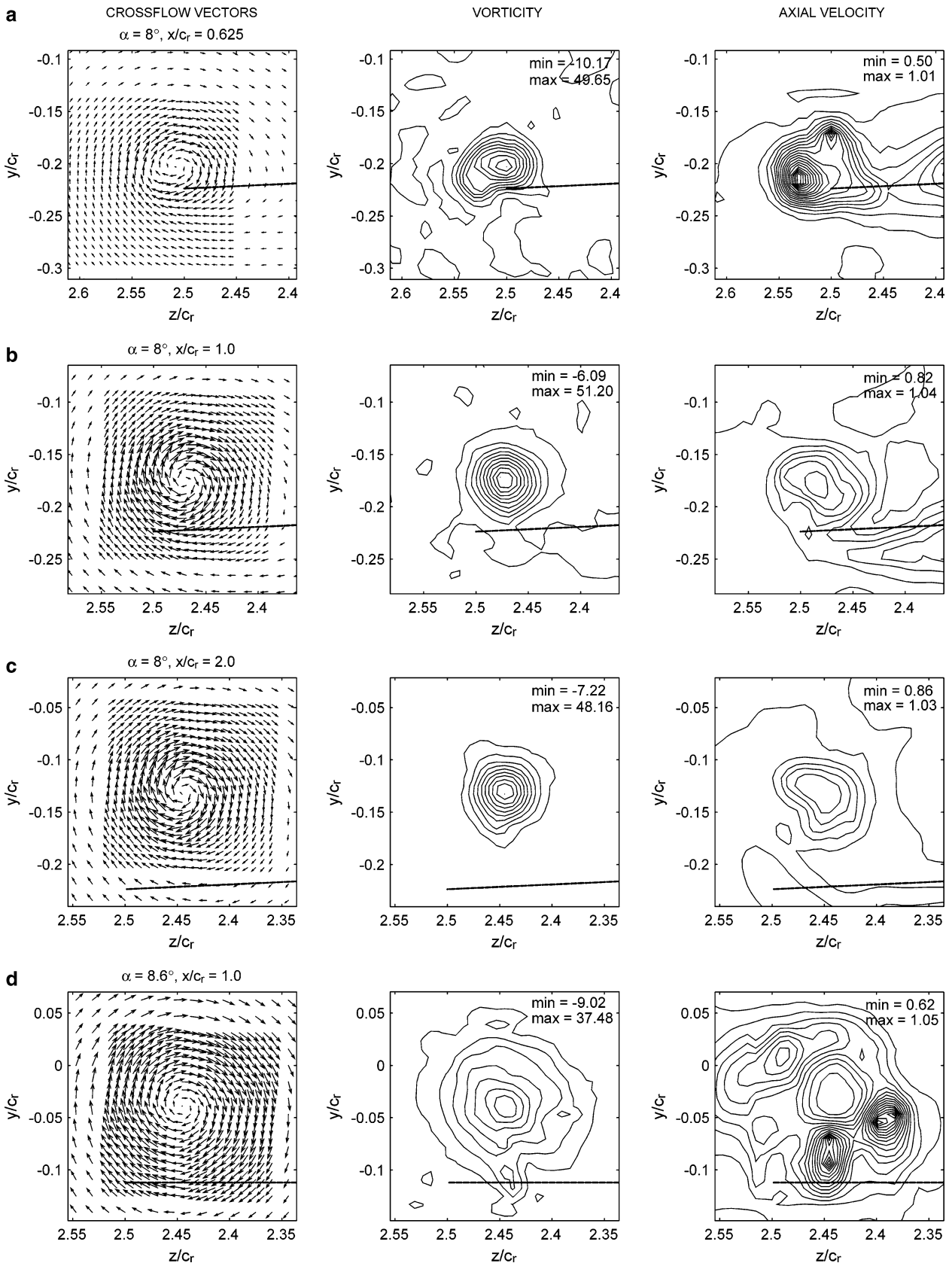
Fig. 3 Typical crossflow vector plots and contours of axial vorticity and velocity. Sweptback and tapered wing at $\alpha = 8°$: **a** $x/c_r = 0.625$, **b** $x/c_r = 1$, and **c** $x/c_r = 2$. **d** Rectangular wing at $x/c = 1$. Numerical values denote u/u_∞ and $\zeta c_r/u_\infty$ levels with constant increments of 0.025 and 5.0, respectively
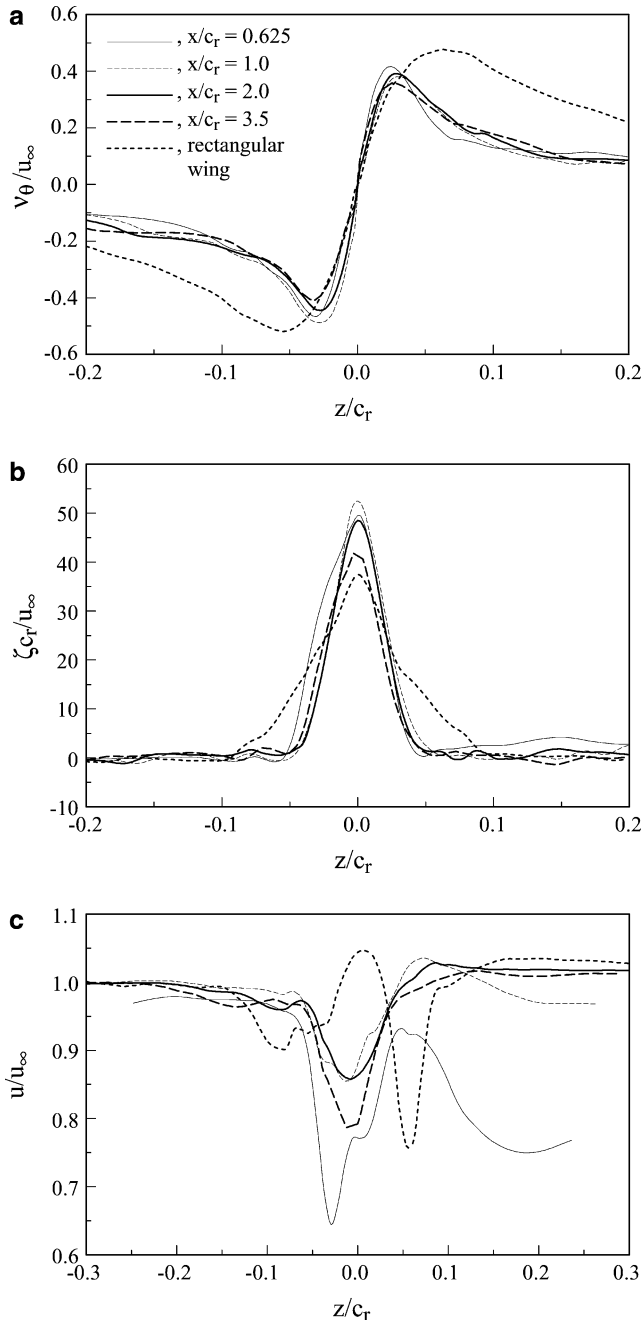
Fig. 4 Vortex flow distributions

in streamwise vorticity), as well as the self-similar behavior observed in the circulation distribution (as discussed in Sect. 3.2). It is known that the axial velocity of the vortex core varies greatly with α and wing loading, and wing geometry, and that it can have "jet-like" or "wake-like" flow conditions (Batchelor 1964; Spalart 1998). Figure 3d shows that for a square-tipped, untwisted rectangular NACA 0015 wing (with AR = 2.5) at the same C_L and Re, the axial velocity distributions were observed to form islands of axial velocity which both exceeded and fell behind the free-stream value, and that the vorticity and vw-velocity structures were found to be

less tightly wound (i.e. with less diffusion) and had lower levels, compared to a sweptback and tapered wing.

Figure 4a–c displays the distributions of the non-dimensional v_θ, ζ, and u about the vortex center for $x/c_r = 0.625$–3.5 at $\alpha = 8°$ Also included in these figures are the rectangular-wing data. All profiles are measured parallel to the z-axis. Similar behavior was also exhibited along the y-axis since a major portion of the vortex flow was only slightly away from being axisymmetric except at $x/c_r = 0.625$. The core-flow region in which v_θ varied nearly linearly from zero to $v_{\theta\max}$ with the radius was identified by the constant slope of the curve (Fig. 4a). At $x/c_r = 0.625$, v_θ was, however, noticeably higher on the suction side by as much as 5%, that is, with $v_{\theta\max}$-$v_{\theta\min} = 0.05u_\infty$, implying an ever-developing vortex. This discrepancy (between $v_{\theta\max}$ and $v_{\theta\min}$) decreased rapidly with downstream distance. For $1 \leq x/c_r \leq 3.5$, the inner region of the tip vortex clearly attained axisymmetry with $v_{\theta\max} = v_{\theta\min}$ within measurement error. Figure 4b shows that for all the x/c_r investigated, the vorticity was highest at the center of the vortex and approached zero outside of the core, and had a bell-shaped wake-like axial velocity distribution (Fig. 4c). The points of minimum velocity deficit clearly coincided with the location of maximum vorticity. The observed wake-like axial velocity profile was attributed to the strong spanwise and outboard directed flow, induced by the sweep and taper of the wing, on the wing upper surface, which led to an early flow separation and well-mixed turbulent wake. Note that for a rectangular wing at the same C_L and Re, the axial flow, however, exhibited a largely wake-like profile mixed with a small jet-like core velocity (of $1.05u_\infty$; Fig. 4c) and was accompanied by a lowered peak vorticity and an increased peak v_θ and core radius, compared to a sweptback and tapered wing.

Figure 5a–e summarizes the variation of the non-dimensional peak values of $v_{\theta\text{peak}}$ and ζ_{peak}, the core axial velocity (or velocity deficit) u_c, the core r_c and outer r_o radii, and the vortex location with x/c_r at $\alpha = 8°$. Also included in Fig. 5a and d is the rectangular-wing data (denoted by dashed and dotted lines). A linear decrease (less than 20%) in the $v_{\theta\text{peak}}$ and ζ_{peak} with increasing downstream distance ($0.625 < x/c_r \leq 2.75$) was observed (Fig. 5a, b); $v_{\theta\text{peak}}$ and ζ_{peak} remained unchanged, within measurement error, for $x/c_r \geq 2.75$. The core axial velocity was observed to vary between $0.64u_\infty$ and $0.86u_\infty$. The core radius (defined by the location of the maximum induced tangential velocity) was, however, found to remain basically unchanged ($r_c = 0.03c_r$ or $0.08c_t$) for $x/c_r > 0.625$, which indicated that the inner flow of the vortex had reached an almost asymptotic state of development. The outer radius r_o (obtained by measuring the extent as the circulation $\Gamma(r_o)$ reached 98% of the total circulation Γ_o) generally increased with the downstream distance; a constant r_o of $0.074c_r$ (or $0.197c_t$), however, was observed for $1.5 \leq x/c_r \leq 2.75$, which rendered a core-radius to outer-radius, r_c/r_o, ratio of about 0.40. Note that due to the relatively asymmetric nature of the tip vortex at $x/c_r = 0.625$, the values of v_θ

Fig. 5 Vortex flow quantities at different x/c_r for $\alpha = 8°$
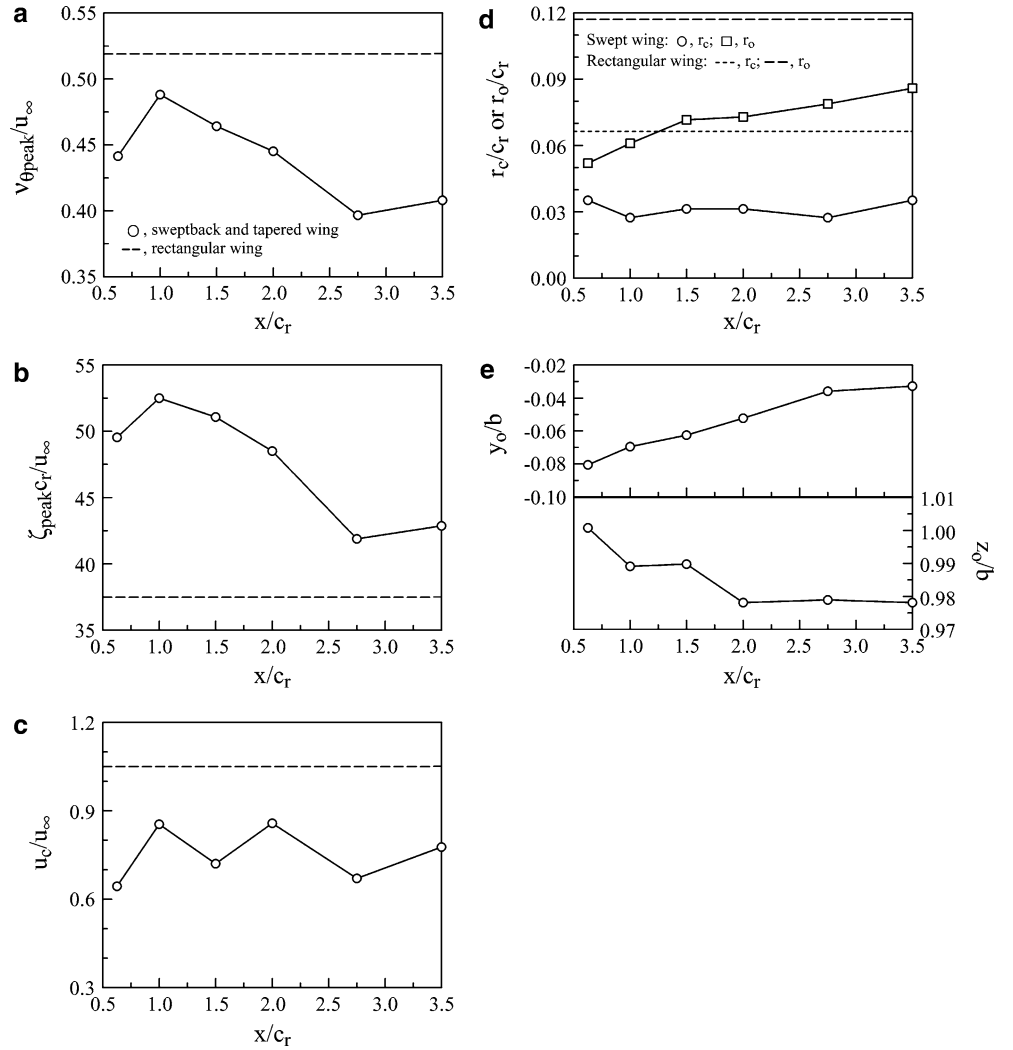
and r_c and r_o shown in Fig. 5a and d at $x/c_r = 0.625$ were circumferentially averaged quantities and thus can only serve as a reference. It is also noteworthy that according to Moore and Saffman (1973), the non-dimensional vortex core radius r_c/c_r is equal to $2.92(x/c_r)^{1/2}Re^{-1/2}$ ($= 0.0054$, 0.0068, 0.0084, 0.0097, and 0.0114 for $x/c_r = 0.625$, 1, 1.5, 2, and 2.75, respectively) for an elliptically loaded wing. The present measurements indicate that the invariant axial change in r_c/c_r ($= 0.03$), once attained axisymmetry of the inner region of the vortex flow, was not proportional to $(x/c_r)^{1/2}$. Figure 5e indicates that, as one would expect, the core was seen to move inboard at a rate that decreased with distance downstream. For the x/c_r range studied, the tip vortex was within $0.05c_r$ (or $0.133c_t$) inboard of the tip edge.

The variation of the vortex flow quantities (i.e. $v_{\theta\text{peak}}$, ζ_{peak}, u_c, and r_c, and r_o) and the vortex trajectory with α at $x/c_r = 2.75$ was also investigated and is presented in Fig. 6a–e. Selected composite plots of the contour maps of $\zeta c_r/u_\infty$ and u/u_∞ for $\alpha = 4$–$10°$ at $x/c_r = 2.75$ are displayed in Fig. 7. It is evident that the axisymmetric distributions (of the inner-flow region) of the vorticity and the wake-like axial velocity also persisted for $\alpha < \alpha_{ss} \approx 10°$ (Fig. 7). For $\alpha \geq 10°$, the tip vortex was disorganized and not discernible. A moderate increase in $v_{\theta\text{peak}}$ and ζ_{peak} for $\alpha \leq 8°$ followed by a reduction for $\alpha > 8°$ was observed (Fig. 6a, b), and was also accompanied by a corresponding decrease and increase in the outer radius and the core axial velocity deficit. The vortex core radius was, however, found to remain unchanged ($r_c = 0.03c_r$) regardless of x/c_r and α for $\alpha < \alpha_{ss}$. No appreciable inboard shifting of the vortex with α was also observed (Fig. 6e).

3.2 Behavior of circulation

The variation of the radial $\Gamma(r)$ and spanwise $\Gamma(z)$ distributions, and the self-similarity of the inner-region circulation of the tip vortex with x/c_r and α is discussed in Figs. 8 and 9. The circulation, or vortex strength, was calculated either by a line integral over the velocity or by the area integral over vorticity. The line integral was evaluated by repeated applications of the trapezoidal rule and was performed on either circular paths or path of constant vorticity. The area integral was evaluated by

Fig. 6 Variation of vortex flow quantities with α for $x/c_r = 2.75$
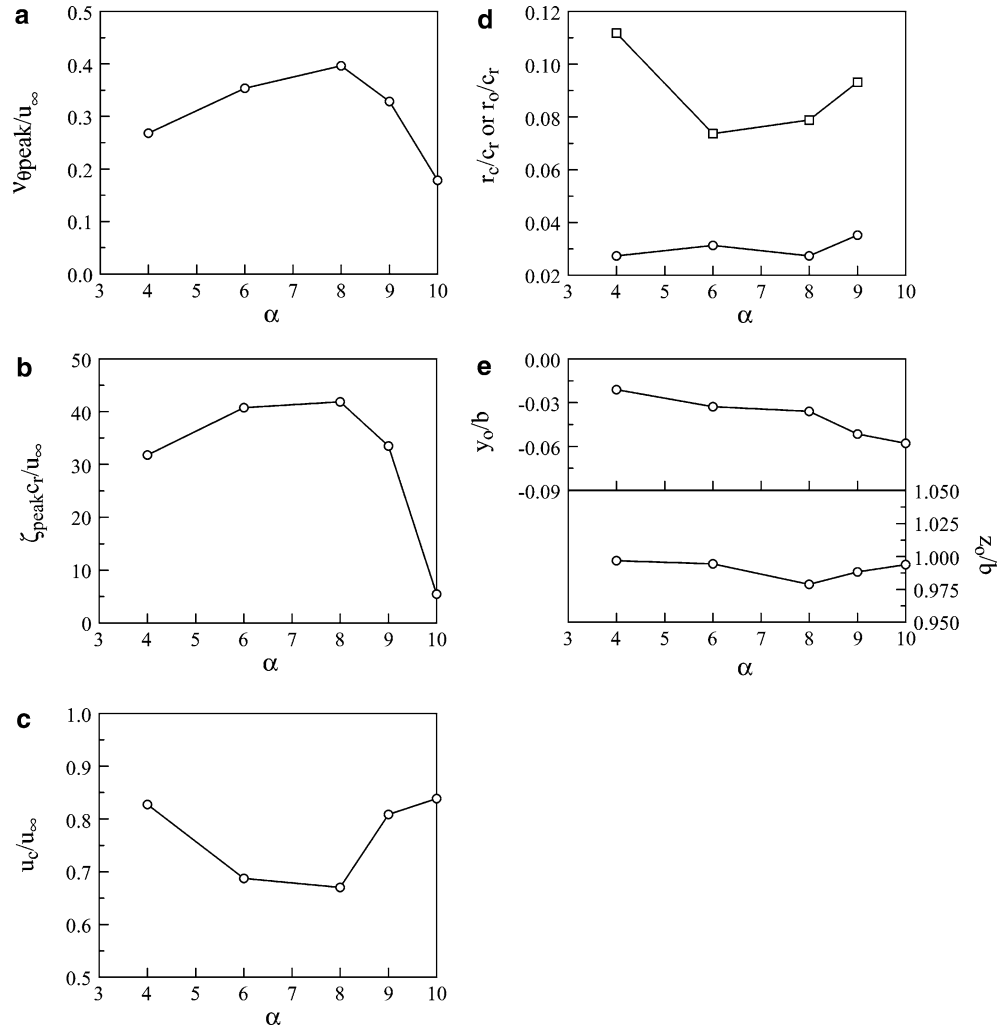
summing the vorticity multiplied with the incremental area of the measuring grid. No noticeable difference was found between these two calculation methods. Figure 8a shows that no noticeable variation was observed in the radial growth and its level of the circulation in the inner-region of the vortex flow with the downstream distance for $1.0 \leq x/c_r \leq 3.5$ studied at $\alpha = 8°$. Also shown in Fig. 8a is the $\Gamma(r)$ distribution of a rectangular wing at the same C_L and Re, which was of a higher vortex strength and had an extended radius compared to a sweptback and tapered wing. Figure 8b indicates that for a sweptback and tapered wing positioned at $\alpha = 8°$ both the core Γ_c and total Γ_o circulation remained somewhat unchanged ($\Gamma_c/u_\infty c_r = 0.069$ and $\Gamma_o/u_\infty c_r = 0.108$, or $\Gamma_c/u_\infty c_t = 0.184$ and $\Gamma_o/u_\infty c_t = 0.288$) for $1.0 < x/c_r \leq 3.5$, implying an almost completion of the roll-up of the tip vortex, especially in the inner region, with a Γ_c/Γ_o ratio of 0.63. The present measurements also indicate a Γ_o/Γ_b ratio of 0.37, suggesting that in the near field (up to $x/c_r = 3.5$, or $x/c_t = 7.6$, tested in the present study) only 37% of the bound root circulation was entrained into the vortex. The bound root circulation Γ_b was determined from:

$$\Gamma_b/u_\infty c_r = \frac{1}{2}(K_1 C_L + K_2), \tag{1}$$

where the constants K_1 and K_2 were determined following the method of Glauert (1926), and $C_L = 0.73$ is the lift coefficient obtained from a force balance (Fig. 10a). It is interesting to note that for a square-tipped rectangular wing at the same lift force and Re conditions, both the core and total circulation had higher values ($\Gamma_c/u_\infty c = 0.195$ and $\Gamma_o/u_\infty c = 0.249$), which rendered a Γ_c/Γ_o ratio of 0.78 (which is consistent with the theoretical value of Γ_c/Γ_o of 0.71 of Lamb's solution (1945), as shown in Fig. 8b by the dashed and dotted lines), and that about 70% of the bound root circulation ($\Gamma_o/\Gamma_b = 0.691$) was entrained into the tip vortex. The variation of Γ_c and Γ_o of the sweptback and tapered with α at $x/c_r = 2.75$ is summarized in Fig. 8c, which indicates that for $\alpha \leq 8°$, the ratios of $\Gamma_c/\Gamma_o = 0.63$ and $\Gamma_o/\Gamma_b = 0.37$ remained basically unchanged.

It is also important to note that the present wake flowfield measurement (up to 85% of the whole span) also allowed the indirect determination of the lift and the bound root circulation from $\Gamma(z)$ distribution. Figure 9a
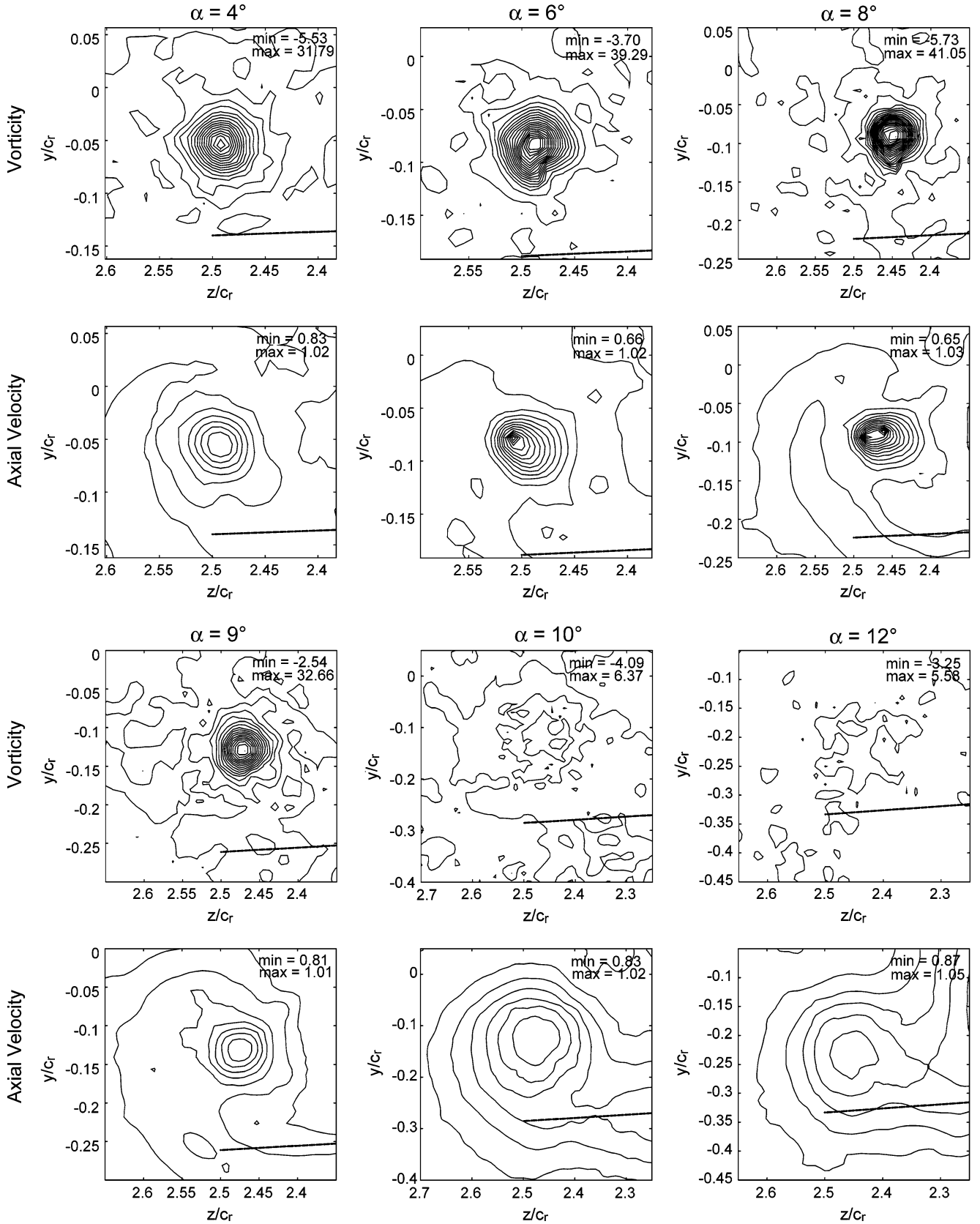
Fig. 7 Composite plots of the axial vorticity and velocity contours at $x/c_r = 2.75$ for $\alpha = 4$–$12°$ Numerical values denote $\zeta c_r/u_\infty$ and u/u_∞ levels with constant increment of 2.0 and 0.025, respectively
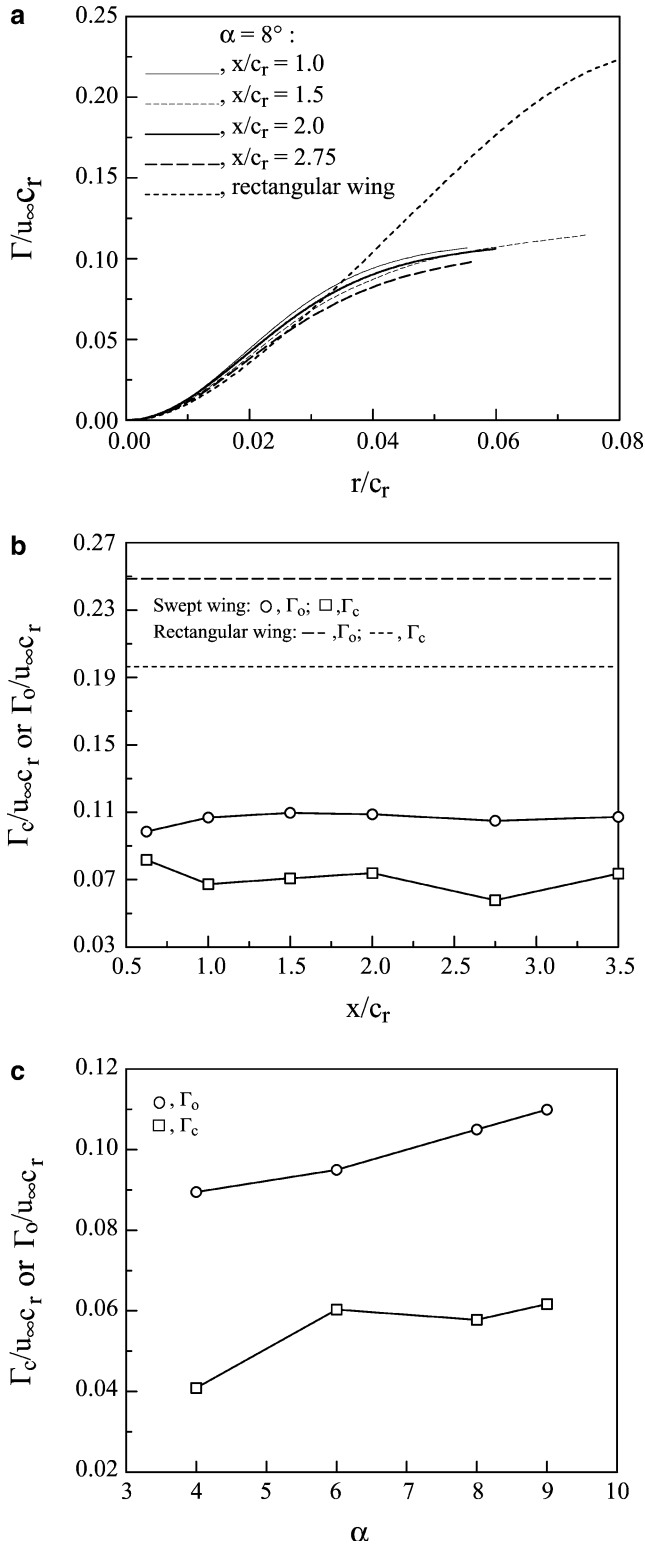
Fig. 8 Radial, core, and total circulation

shows the variation of $\Gamma(z)$ with the spanwise location z, normalized by the (semi-)wing span b, with x/c_r at $\alpha = 8°$ Also shown in Fig. 9a are the $\Gamma(z)$ distributions for an elliptical wing loading and a square-tipped rectangular wing at the same C_L and Re. The results show that for a

sweptback and tapered wing, no significant difference in the spanwise circulation distributions in the near field was observed; an average non-dimensional bound root circulation $\Gamma_{b,m}/u_\infty c_r$ of about 0.32 was obtained at $z = 0$ or at the root of the half-wing model tested. The measured bound circulation $\Gamma_{b,m}$ was found to be about 10% lower than the bound root circulation determined from the classical inviscid lifting-line theory $\Gamma_b/u_\infty c_r = \frac{1}{2}(K_1 C_L + K_2) = 0.352$ at $C_L = 0.73$. Figure 9a also reveals that for a sweptback and tapered NACA 0015 wing (with an AR of 3.654 and a λ of 0.375), there was a dip in the spanwise $\Gamma(z)$ distribution near the tip at $\alpha = 8°$. For a rectangular wing, however, no noticeable difference was observed between the measured $\Gamma_{b,m}$ and the bound root circulation computed from Eq. 1. Also, more lift force was generated in the rectangular-wing tip region, implying a tip vortex of stronger vortex strength and higher lift-induced drag (as indicated in Figs. 8b, 12a), compared to an elliptically loaded wing as well as the sweptback and tapered wing tested. The spanwise $\Gamma(z)$ distributions of the sweptback and tapered wing for $\alpha = 4$, 6, 8, 10, 11, and 12° at $x/c_r = 2.75$ were also computed and are presented in Fig. 9b. Special attention, however, should be given to the behavior of $\Gamma(z)$ near the tip region as well as its level close to the root at large angles of attack (i.e. for $\alpha > 10°$). For $\alpha \leq 10°$ the $\Gamma(z)$ distribution near the tip was more gradual. At $\alpha = 11$ and 12° ($> \alpha_{ss}$), the dip in the near-tip $\Gamma(z)$ distribution was found to be more precipitous and shifted further inboard with a drastically increased Γ level close to the root of the wing model. Comparisons among the lift coefficients determined from the measured bound root circulation $\Gamma_{b,m}$ [i.e. $C_L = 2\Gamma_{b,m}/K_1 u_\infty c_r - K_2/K_1$ via Eq. 1], the wind-tunnel force balance, and the integral of $\Gamma(z)$ through the lifting-ling theory:

$$L = \rho_\infty u_\infty \int_{-b/2}^{b/2} \Gamma(z) \, dz \qquad (2)$$

are summarized in Fig. 10c and d. L is the total lift ($= \frac{1}{2}\rho_\infty u_\infty^2 S C_L$, where ρ_∞ is the density of the freestream).

Figure 10a shows that for a rectangular NACA 0015 wing without tip effects at $Re = 1.81 \times 10^5$, the lift curve (of a slope $dC_L/d\alpha$ of 0.124) was rather sharp-peaked in the vicinity of C_{Lmax} ($= 1.21$) with a rapid decrease in C_L above the stall ($\alpha_{ss} = 14°$, and that the stalling mechanism was of a leading-edge stall type. For a 3-D wing configuration, the values of $dC_L/d\alpha$, C_{Lmax}, and α_{ss}, were found to be 0.092, 1.02, and 15°, respectively, and the stalling mechanism remained unchanged. For the sweptback and tapered wing tested, the stall was, however, found to be a very "soft" trailing-edge stall, which yielded a gradual bending-over of the lift curve (with $\alpha_{ss} \approx 10°$, $C_{Lmax} = 0.8$, and $dC_L/d\alpha = 0.136$), in contrast to the sharp precipitous drop in C_L of a rectangular wing. No significant difference in the lift-curve slope, C_{Lmax} and the static-stall angle, as well as in C_D (Fig. 10b) was
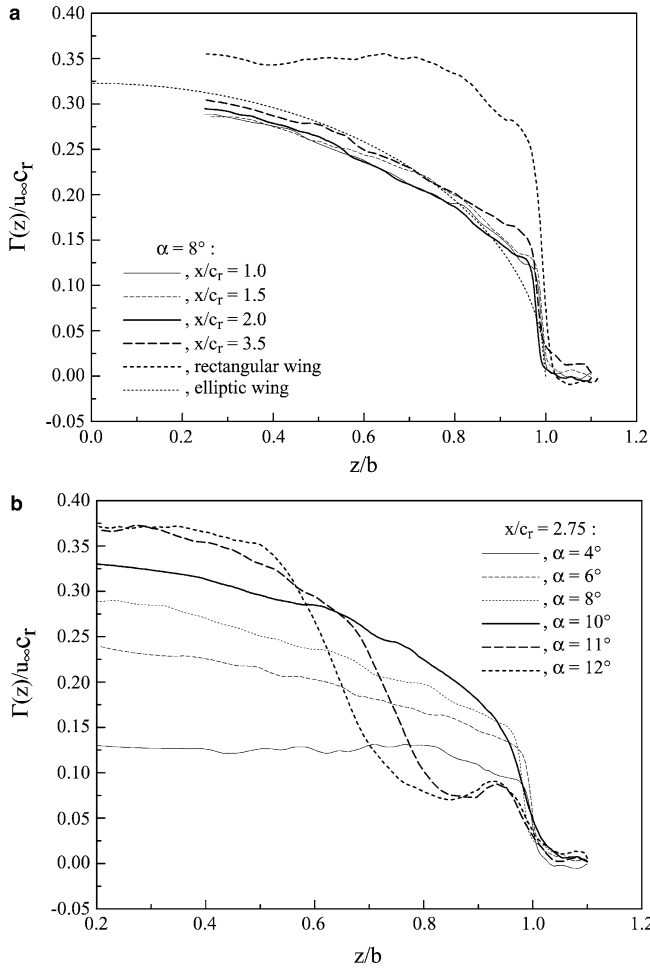
a

b

Fig.9 Spanwise circulation distributions

observed for a sweptback and tapered wing model with and without tip effects. Figure 10c and d presents the values of C_L, determined from Eq. 2 and also $\Gamma_{b,m}$ (i.e. $C_L = 2\Gamma_{b,m}/K_1 u_\infty c_r - K_2/K_1$) at different downstream distances for $\alpha = 8°$ and airfoil incidence for $x/c_r = 2.75$, respectively. The lift coefficients determined from Eq. 2 were in reasonable agreement with the force-balance measurements, indicating that the circulation distributions were consistent with the measured lift data according to the Kutta–Joukowsky theorem. The lift coefficients computed from the measured bound root circulation $\Gamma_{b,m}$, in conjunction with Eq. 1, however, underestimated the C_L values to a greater extent compared to those of Eq. 2.

The present measurements also show that the radial distribution of $\Gamma(r)$ of a sweptback and tapered wing, normalized by Γ_c, plotted against $\log(r/r_c)$ also shows some interesting characteristics for $1.0 \leq x/c_r \leq 3.5$. Figure 11a indicates that at $x/c_r = 2.75$, the distribution of $\Gamma(r)$ within the tip vortex core followed a $\Gamma \propto r^2$ profile for $r/r_c < 0.4$ and varied logarithmically for $0.5 < r/r_c < 1.4$; a phenomenon similar to that of a rectangular wing (Ramaprian and Zheng 1997; Birch and Lee 2004). For $r/r_c > 1.4$, $\Gamma(r)$ continued to vary with x/c_r and α,

suggesting that at $r > 1.4 r_c$, the roll-up of the vortex was only nearly complete and there was a slow addition of vorticity (as much as 63% of Γ_b) to the outer layers of the vortex from the shear layer arriving from the inboard regions. Note that as discussed previously, the tip vortex accounted for 37% of the bound root circulation for a sweptback, tapered NACA 0015 wing with an AR of 3.654 and a λ of 0.375. The observed self-similar behavior of the inner region of a nearly axisymmetric tip vortex in the near-wake region is of particular interest since it generally takes a distance of several tens or even hundreds of wing chords downstream for the vortex to become fully developed and attain the characteristics of asymptotic trailing vortices. The empirical curve-fit relationships that describe the inner-core region and the region where the $\Gamma(r)$ distribution is logarithmic, according to Hoffman and Joubert (1963) and Phillips (1981) are

$$\Gamma(r)/\Gamma_c = A(r/r_c)^2 \quad \text{for} \quad r/r_c < 0.4, \tag{3}$$

$$\Gamma(r)/\Gamma_c = B \log(r/r_c) + C \quad \text{for} \quad 0.5 < r/r_c < 1.4. \tag{4}$$

The curve-fit constants obtained at different x/c_r are listed in Table 1. Furthermore, for $0.625 < x/c_r \leq 3.5$, all the data within $0 < r/r_c < 1.2$ collapsed together onto a sixth-order polynomial (similar to that reported by Ramaprian and Zheng 1997; Birch and Lee 2004) with a self-correlation coefficient of 0.998:

$$\Gamma(r)/\Gamma_c = 1.756(r/r_c)^2 - 1.044(r/r_c)^4 + 0.263(r/r_c)^6. \tag{5}$$

Figure 11b compares the present self-similar inner-flow structures of a tip vortex in the near field of a sweptback and tapered wing at $\alpha = 8°$ with those of Hoffman and Joubert (1963) and Ramaprian and Zheng (1997). It is clear that the present measurements are in good agreement with the published results. Moreover, in addition to the observed constant ratios of $r_c/r_o = 0.41$, $\Gamma_c/\Gamma_o = 0.63$, and $\Gamma_o/\Gamma_b = 0.8$ for $\alpha < 9°$, the self-similar behavior of the inner flow of the vortex also persisted. The curve-fit coefficients of Eqs. 3 and 4 as a function of α are listed in Table 1.

3.3 Lift-induced drag

The lift-induced drag coefficient C_{Di} was also computed, based on the vorticity inferred from the measured velocity field, by using the Maskell induced-drag model (Maskell 1973) at different downstream distances for $\alpha = 8°$ (Fig. 12a). The vw-crossflow velocity vectors within the measurement plane were decomposed into a stream function $\psi(y, z)$ and a velocity potential $\phi(y, z)$ with the imposed boundary conditions requiring both ψ and ϕ to be zero on the edges of the measurement plane. The lift-induced drag was then obtained by
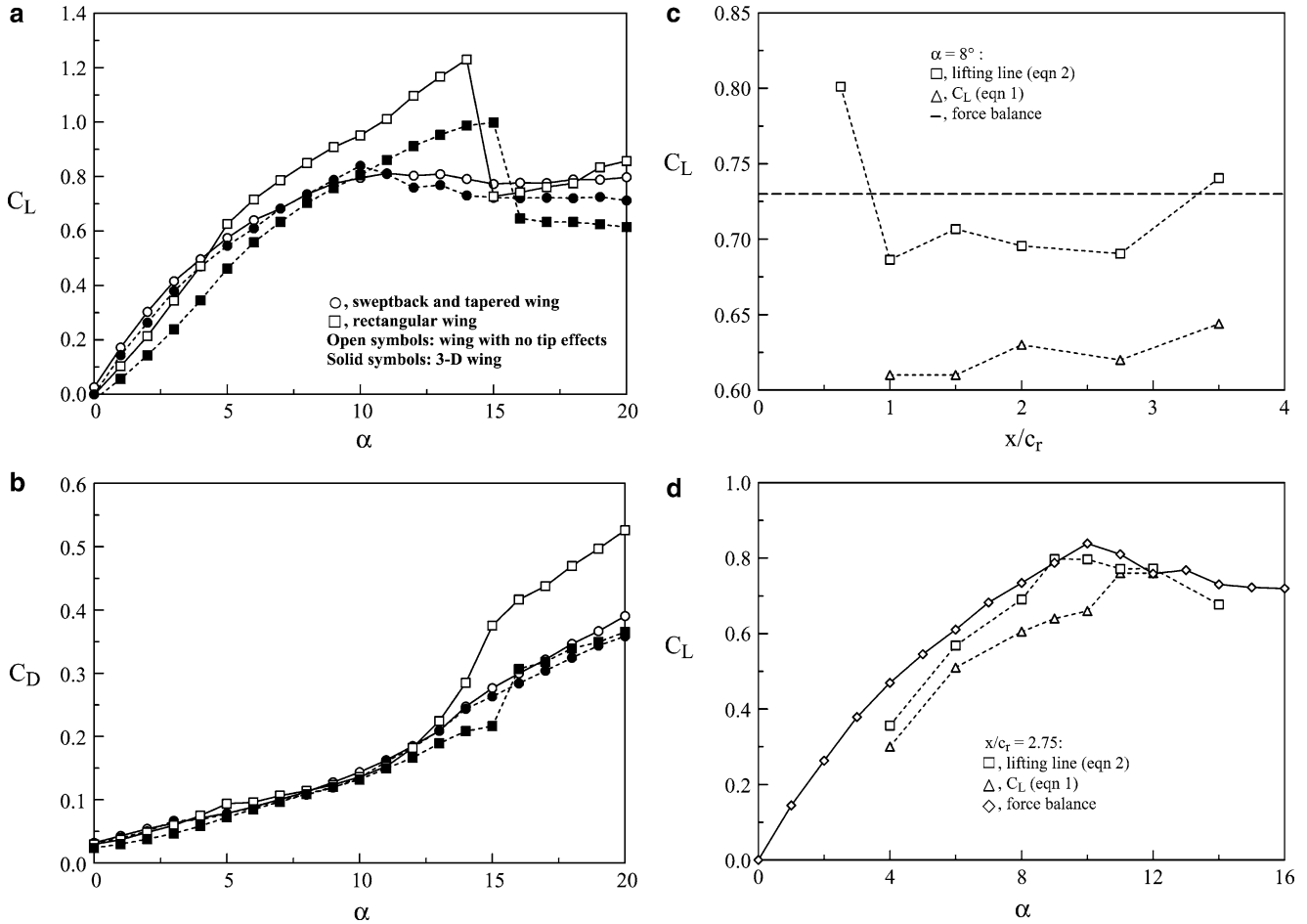
Fig. 10 Lift and drag coefficients

$$D_i = \frac{1}{2}\rho_\infty \iint\limits_{s_\zeta} \psi\zeta\,\mathrm{d}y\,\mathrm{d}z - \frac{1}{2}\rho_\infty \iint\limits_{s1} \phi\sigma\,\mathrm{d}y\,\mathrm{d}z, \qquad (6)$$

where ζ is the vorticity, the surface S_ζ is the region within $S1$ where the vorticity is nonzero, $\sigma\ (=\partial v/\partial y + \partial w/\partial z)$ is a source term, and the flow is incompressible. Figure 12a shows that similar to the observed evolution of $v_{\theta\mathrm{peak}}$ and ζ_{peak} with the downstream distance (Fig. 5a and b) at $\alpha = 8°$, the lift-induced drag coefficient of a nearly axisymmetric vortex also presented a local maximum (with a $C_{Di} = 0.0026$ at $x/c_\mathrm{r} = 1.0$ and decayed slowly to $C_{Di} = 0.0023$ at $x/c_\mathrm{r} = 3.5$, compared to $C_{Di} = 0.0055$ for a rectangular wing at the same C_L and Re with $x/c_\mathrm{r} = 1$. Also shown in Fig. 12a are the C_{Di} obtained from:

$$D_i = \iint\limits_{s2} \frac{1}{2}\rho_\infty(v^2 + w^2)\,\mathrm{d}y\,\mathrm{d}z, \qquad (7)$$

as suggested by Brune (1994) and Kusunose (1997). It can be seen that the results calculated by Eq. 7 were generally 25% higher than those obtained with Eq. 6 except at $x/c_\mathrm{r} = 2.75$ and 3.5.

Figure 12b indicates that the C_{Di}, computed by using Eqs. 6 and 7 at $x/c_\mathrm{r} = 2.75$, increased with α (for $\alpha < \alpha_{\mathrm{ss}}$).

Also shown in Fig. 12a and b are the C_{Di} values determined from the following two inviscid lifting-line equations:

$$C_{Di} = C_L^2/(K + \pi e \mathrm{AR}_{\mathrm{eff}}), \qquad (8)$$

and the Prandtl's lifting-line theory

$$D_i = L\sin\alpha_i = L\sin\alpha_i(z_0) = \frac{1}{4\pi U_\infty} \int\limits_{-b/2}^{b/2} \left(\frac{\frac{\mathrm{d}\Gamma}{\mathrm{d}z}\,\mathrm{d}z}{z - z_0}\right)\cdot L, \tag{9}$$

where K is the pressure drag magnification factor and has a typical value of 0.007 (Naik and Ostowari (1990)), $e = 0.9$ is the Oswald wing span efficiency factor, $\mathrm{AR}_{\mathrm{eff}} = 2\mathrm{AR} = 7.308$, L is the total lift, and α_i is the lift-induced angle of attack. Note that the Prandtl's classical inviscid lifting-line theory overpredicted the lift-induced drag; an order of magnitude larger than those computed from Eqs. 6 and 7 was observed. The discrepancy in the C_{Di} values determined from the measured crossflow vorticity and the lifting-line theory could be attributed to the fact that the lifting-line theory may not be applied successfully due to the low Reynolds number and the

Table 1 Curve-fit constants of Eqs. 3 and 4

x/c_r ($\alpha = 8°$)				α ($x/c_r = 2.75$)			
	A	B	C		A	B	C
0.625	1.274	2.700	1.012	4°	1.493	2.290	0.996
1.0	1.656	2.081	0.984	6°	1.690	2.103	0.983
1.5	1.473	2.240	0.987	8°	1.361	2.338	0.988
2.0	1.428	2.301	0.990	9°	1.864	2.030	0.996
3.5	1.427	2.282	0.995				

small AR, and that in the near field downstream from the trailing edge not all the bound vorticity generated over the wing has been aligned in the downstream flow direction. Nevertheless, the continuous increase in the value of C_{Di} with α, determined by Eq. 9, for $\alpha > \alpha_{ss}$ is particularly disturbing.

4 Conclusions

The three-dimensional near-field mean flow structure of a tip vortex behind a sweptback and tapered NACA

0015 wing with an AR of 3.654 and a λ of 0.375 was investigated at $Re = 1.81 \times 10^5$. The peak tangential velocity and vorticity were found to increase with x/c_r and decreased with α, for $\alpha \leq 8°$. The core radius was about $0.03c_r$ or $0.08c_t$, regardless of the increase in α and the downstream distance. The core and overall circulation of the tip vortex remained nearly constant up to $x/c_r = 3.5$ with Γ_c/Γ_o and Γ_o/Γ_b equal to 63 and 37%, respectively. The axial velocity profiles were always wake-like. For a square-tipped rectangular wing of an AR of 2.5 at the same lift force and Re, the axial flow was found to have islands of wake- and jet-like velocity distributions even through the majority of the vorticity distribution had attained axisymmetry for $x/c \geq 0.5$.
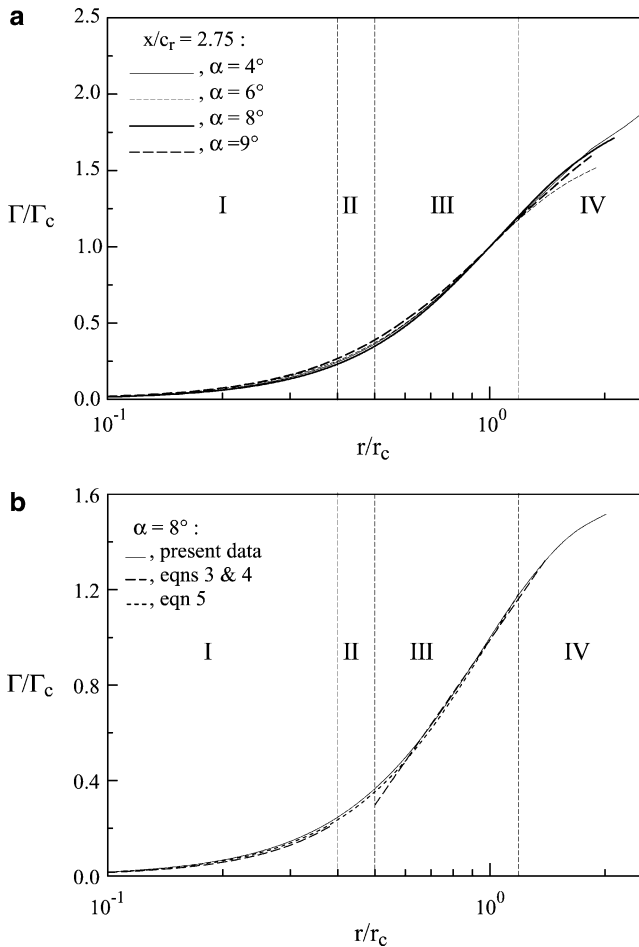
Fig. 11 Behavior of inner-region circulation. *I* inner-core region, *II* buffer region, *III* logarithmic region, and *IV* outer region
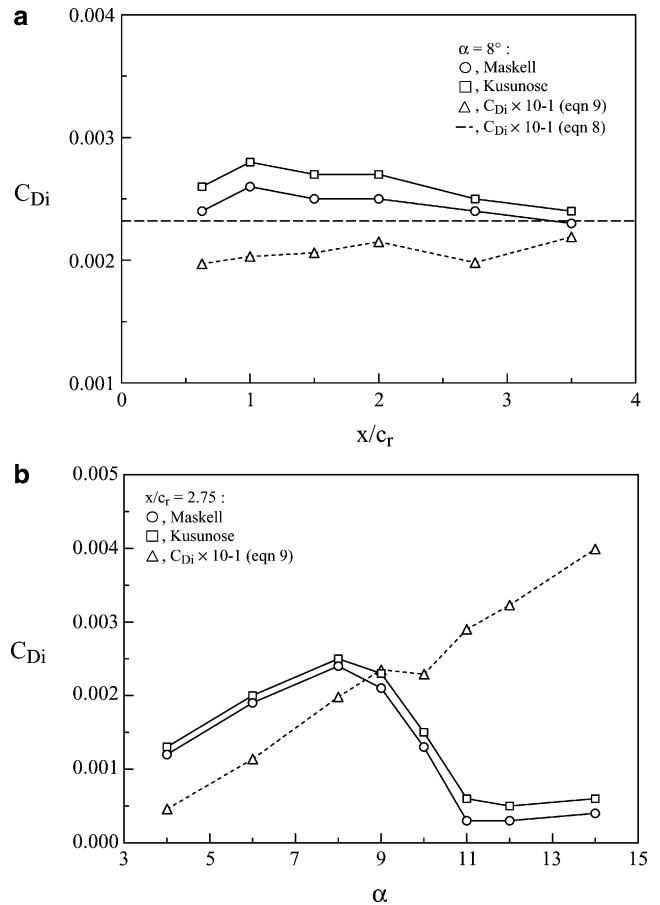
Fig. 12 Lift-induced drag coefficients

About 70% of the bound root circulation Γ_b was entrained into the tip vortex in the near field behind a rectangular wing. In addition, for a sweptback and tapered wing, the self-similar behavior of the inner flow of the vortex was observed for $x/c_r \geq 1.0$. The lift-induced drag coefficients, computed from the vorticity field inferred from the crossflow measurements, were found to fall well below the values estimated by the classical inviscid lifting-line theory.

References

Batchelor GK (1964) Axial flow in trailing line vortices. J Fluid Mech 20:645–658

Birch D, Lee T (2004) Structure and induced drag of a tip vortex. J Aircr 41(5):1138–1145

Brune GW (1994) Quantitative low-speed wake surveys. J Aircr 31(2):249–255

Chow JS, Zilliac GG, Bradshaw P (1997) Mean and turbulence measurements in the near field of a wingtip vortex. AIAA J 35(10):1561–1567

Devenport WJ, Rife MC, Liapis SI, Follin GJ (1996) The structure and development of a wing-tip vortex. J Fluid Mech 312:67–106

El-Ramly Z, Rainbird WJ, Earl DG (1976) Wind tunnel measurement of rolling moment in a swept-wing vortex wake. J Aircr 13(12):962–967

Francis MS, Kennedy DA (1979) Formation of a trailing vortex. J Aircr 16(3):148–154

Francis TB, Katz J (1988) Observations on the development of a tip vortex on a rectangular hydrofoil. J Fluids Eng 110:208–215

Glauert TH (1926) The elements of airfoil and airscrew theory. Cambridge University Press, London

Green SI, Acosta AJ (1991) Unsteady flow in trailing vortices. J Fluid Mech 227:107–134

Hoffmann ER, Joubert PN (1963) Turbulent line vortices. J Fluid Mech 16:395–411

Kusunose K (1997) Development of a universal wake survey data analysis code. AIAA 2294

Lamb H (1945) Hydrodynamics, 6th edn. Dover, New York, p 592

Maskell E (1973) Progress towards a method for the measurement of the components of the drag of a wing of finite span. RAE Technical Report 72232

McAlister KW, Takahashi RK (1991) NACA 0015 wing pressure and trailing vortex measurements. NASA TP-3151

Moore DW, Saffman PG (1973) Axial flow in laminar vortices. Proc R Soc Lond A 333:491–508

Naik DA, Ostowari C (1990) Effects of nonplanar wing forms on a wing. J Aircr 27(2):117–122

Orloff KL, Ciffone DL (1974) Vortex measurements behind a swept wing transport model. J Aircr 11(6):362–364

Ozger E, Schell I, Jacob D (2001) On the structure and attenuation of an aircraft wake. J Aircr 38(5):878–887

Phillips WRC (1981) The turbulent trailing vortex during roll-up. J Fluid Mech 105:451–467

Ramaprian BR, Zheng Y (1997) Measurements in rollup region of the tip vortex from a rectangular wing. AIAA J 35(12):1837–1843

Shekarriz A, Fu TC, Katz J, Huang TT (1993) Near-field behavior of a tip vortex. AIAA J 31(1):112–118

Spalart PR (1998) Airplane trailing vortices. Ann Rev Fluid Mech 30:107–138

Wenger CW, Devenport WJ (1999) Seven-hole pressure probe calibration utilizing look-up error tables. AIAA J 37(6):675–679

Williams GM (1974) Viscous modeling of wing-generated trailing vortices. Aeronaut Q 25:143–154

Zeman O (1995) The persistence of trailing vortices: a modeling study. Phys Fluids 7(1):135–143